Absolute cross section for loss of supercoiled topology induced by 10 eV electrons in highly uniform /DNA/1,3-diaminopropane films deposited on highly ordered pyrolitic graphite.

Omar Boulanouar, Michel Fromm, Andrew D Bass, Pierre Cloutier, Leon Sanche

Absolute cross section for loss of supercoiled topology induced by 10 eV electrons in highly uniform /DNA/1,3-diaminopropane films deposited on highly ordered pyrolitic graphite

Omar Boulanouar[1], Michel Fromm[1], Andrew D. Bass[2*] , Pierre Cloutier[2], Léon Sanche[2]

[1] Laboratoire de Chimie Physique et Rayonnements – Alain Chambaudet, LRC CEA, UMR CNRS 6249, Université de Franche-Comté, 16 route de Gray, F-25030 Besançon cedex, France

[2] Groupe en Sciences des Radiations, Département de Médecine Nucléaire et de Radiobiologie, Faculté de Médecine et des Sciences de la Santé, Université de Sherbrooke, Québec, J1H 5N4, Canada

Abstract:

It was recently shown that the affinity of doubly-charged, 1-3 diaminopropane (Dap^{2+}) for DNA permits the growth on highly ordered pyrolitic graphite (HOPG) substrates, of plasmid DNA films, of known uniform thickness [Boulanouar et al., J. Phys. Chem. C. 115, 21291 (2011)]. Post-irradiation analysis by electrophoresis of such targets confirms that electron impact at 10 eV produces a maximum in the yield of single strand breaks that can be associated with the formation of a DNA^- transient anion. Using a well-adapted deterministic survival model for the variation of electron damage with fluence and film thickness, we have determined an absolute cross section for strand-break damage by 10 eV electrons and inelastic scattering attenuation length in DNA-Dap complex films.

[*] Corresponding Author ; Andrew.Bass@Usherbrooke.ca

I. INTRODUCTION

The physico-chemical processes initiated by the transfer of energy from *primary* ionizing radiation to condensed media proceed via the production of *secondary* species that include large numbers of secondary electrons (SE) as well as ions, radicals and excited atoms and molecules. These species form along the radiation *tracks* created by the primary charged particles or primary electrons[1]. Their yields, temporal and spatial evolution and the reactions they induce, can be described by detailed history Monte Carlo (MC) simulations[2,3] that follow event-by-event, their slowing down. The accuracy of simulations thus depends on data describing individual scattering events, e.g., those of SE with condensed molecules. Electron-molecule cross sections are *absolute* quantities that describe these events and are thus essential for modelling radiation induced processes occurring in diverse fields including plasma processing[4], water e-beam purification[5], astro-chemistry[6], human spaceflight[7] and radiobiology.[8]

In radiobiology, MC simulations can describe both the so-called *direct effects* of primary radiation and secondary species on DNA, as well as the *indirect effects* of $OH^{\cdot}$ and other radicals produced in liquid water.[2,3] Indeed, most studies focus on describing processes occurring in water, which is an important component of living matter and for which experimental and theoretical cross sections are readily available.[2,3] Other relevant targets, like molecular DNA, alone or bound into complex structures with proteins, can be superimposed over the liquid water track structure[9] and the direct effect of radiation estimated from the energy deposited within their molecular volume.[9,10] Recent, detailed MC calculations of clustered DNA damage (i.e, combinations of multiple strand breaks and base lesions) include cross section data for the DNA (and/or its sub-units)[11]. Since MC simulations follow events down to the lowest energies and since low energy

electrons (LEEs) with energies < 30 eV represent the majority of SE, simulation accuracy strongly depends on LEE--molecule scattering cross sections. Ionization and excitation cross sections at high electron energies (E > 10 keV) are calculable via the plane wave Born approximation[10] or by modeling the dielectric response function.2 At lower energies *semi-empirical* models (often using chemical structure codes such as GAMESS and GAUSSIAN) have been used to calculate total inelastic electron impact cross sections for bio-organic compounds such as DNA and RNA bases and other DNA sub-units[12,13,14,15]. Such methods can generate accurate data for electron energies above 100 eV, but are much less reliable at energies typical of LEE. So far, the only *experimentally* derived, absolute LEE cross sections for inclusion in MC simulations are those measured for amorphous water ice.[16,17] There exists a dearth of experimentally derived data for damage to what is arguably, the most important target in radiobiology, the DNA molecule.

Despite recent success with larger DNA sub-units (e.g., thymidine and d-ribose-5-phosphate) and with short synthetic oligonucleotides[18,19] it is not possible to vaporize DNA for gas-phase electron-molecule impact experiments. Thus, *effective* LEE-molecule cross sections have been obtained from thin film experiments performed under ultra high vacuum (UHV) conditions. Such experiments are problematic; electrons incident on solid targets undergo multiple collisions, in which an uncertain number of ill-defined energy quanta are transferred. Moreover, the preparation of biological DNA films by techniques such as lyophilisation is challenging; with high purity *plasmid* DNA it is difficult to produce films of uniform thickness and morphology[20,21] suitable for the cross section measurement and such films are prone to charging, which limits the penetration of

LEEs[22]. While measurement of LEE induced damage under such conditions is possible (e.g., refs [23,24,25,26]), and has even allowed measurement of more transferable cross sections[22], by varying film thicknesses, there exists a need for absolute cross sections for DNA damage induced by LEEs. Such values can be derived from experiments on uniform plasmid DNA films, which can be recovered from their substrate for post-irradiation analysis.

Polyamine cations can stabilize the negative charge along the sugar-phosphate backbone[27], participate in DNA folding-unfolding[28] and when complexed to C_8-alkyl molecules, aid the formation of a hydrophobic layer around DNA[29]. Recently, we described a method to produce DNA films of uniform and directly measurable thicknesses on conductive substrates of highly ordered pyrolitic graphite (HOPG)[30]. The technique employs the diamine, 1,3-diaminopropane in its doubly-protonated form at neutral pH (Dap^{2+}, Figure 1a), to bind plasmid DNA molecules to the HOPG and to each other (Fig 1b). The film thickness can varied between 1 and 10 ML by controlling the concentration of plasmid DNA (C_{DNA}) and the molar ratio of Dap^{2+} ions to phosphate sub-units ($R = [Dap^{2+}]/[PO_4^-]_{DNA}$). Significantly, all but the first monolayer, which has a thickness of 2.2nm and is tightly bound to the substrate, can be removed by washing for post-irradiation analysis.[30]

Here, we employ the new preparation method[30] to fabricate DNA samples for electron irradiation experiments in ultra high vacuum (UHV). Post-irradiation analysis of recovered DNA/Dap^{2+} plasmids that were bombarded by 4 to 14 eV electrons reveals a maximum in the loss of super-coiled DNA at an impact energy of 10 eV, similar to earlier reports[23]. Exposure response data obtained at this energy with films of three

different thicknesses further allow the measurement of an absolute cross section for electron induced strand-breaks . This measurement is in large part possible because of the high uniformity of sample films and the consequently limited film charging during irradiation. Below, we describe the preparation and characterisation of the DNA-Dap^{2+} films. Subsequently, we present our experimental results and a simple model of electron transmission. The results are discussed in relation to previous experimental and theoretical cross sections for strand break damage.

II. EXPERIMENTAL

A. Chemicals

Sample films were prepared using plasmid DNA (pUC21, 3151bp, from PlasmidFactory GmbH & Co. KG (Germany)) at an initial concentration of 1mg/ml in the presence of a TRIS/EDTA buffer (to maintain DNA integrity)[30]. Without further purification, a stock solution of the pUC21 DNA (>95% supercoiled) was prepared by dilution in ultrapure water (resistivity of 18.2 M Ω.cm). The DNA concentration was determined by measuring the absorbance at 260 nm using the molar extinction coefficient ε_{260} = 5.3 x 10^7 cm^{-1} M^{-1}.[31] 1,3-Diaminopropane Dihydrochloride (98%) was purchased from Sigma-Aldrich and kept at 4°C. Films were formed on HOPG (ZYA grade, NT-MDT) substrates according to the protocol described in ref 30.

B. DNA deposits characterization

Film thickness was controlled by varying C_{DNA}; to obtain 5, 7.5 and 10 ML DNA-Dap films, solutions of plasmid DNA at 200, 300 400 ng/µl, respectively, were mixed

with equal volumes of a solution containing Dap^{2+} to attain a ratio R=16. The concentrations of Dap^{2+} in the solutions used to obtain these dense films are thus much greater than those of DNA phosphate groups. However, XPS measurements of similar DNA-Dap^{2+} films formed without TE buffer by the same deposition process, but with R equal to 8, 16 and 32 and C_{DNA} fixed at 20 ng/µl, show that the number of Dap^{2+} ions per DNA phosphate group in the films only varies from 1.25 to 1.75.[32] Film composition is thus nearly independent of R and far more dependent on the interactions between the HOPG, Dap^{2+} ions and DNA, that precipitate out the DNA/Dap^{2+} complexes. It is likely that this latter observation is also applies to the present films

Some samples were characterized by atomic force microscopy (AFM) and others immediately introduced in the UHV chamber for LEE irradiation. The AFM images were obtained in air at standard ambient temperature and pressure, using a Molecular Imaging (now, Agilent) scanning probe microscope operated with aluminium coated, silicon nitride tips (Nanoandmore), at a contact/tapping mode (AFM Scratching) resonant frequency of 300 kHz.

C. DNA exposition to electrons and damage analyses

After degassing for 24hrs at room temperature and pressure of 2×10^{-8} Pa, samples were subjected to electron irradiation as described elesewhere[24,26]. Samples (of area 19.0 ± 0.5 mm^2) were irradiated in UHV sequentially, for periods of between 0 and 8 minutes, at selected energies. The electron beam had a cross sectional area of 8± 1 mm^2-The incident current was set at 5 nA, so that the current density J_0 was 0.39 $x10^{12}$ electrons s^{-1} cm^{-2}.

After irradiation, samples were removed from UHV and immediately dissolved in 20µl of ultrapure water. The separation of the recovered DNA into the undamaged super-coiled (SC), nicked circular (C) and linear (L) structural forms was performed by agarose gel electrophoresis[24],[26]. The DNA samples and the agarose gels were stained with SYBR Green I in concentrations of x100 and x10000, respectively. The samples were passed on 1% agarose gel Tris—acetic acid—EDTA (TAE) buffer at 100 V for 7 min, then at 75 V for 68 min (5 Vcm−1). Gels were scanned by a Typhoon-Trio laser scanner (GE Healthcare), using the blue fluorescent mode at 488 nm and filter type 520 nm band pass (520 BP 40) in the normal sensitivity mode. The fraction of each DNA structural form were analysed by IMAGEQUANT (Molecular Dynamics) software.

III. RESULTS AND DISCUSSION

A. Film thickness

The film thickness was determined by AFM as illustrated in Figure 2a for a 5 ML (11nm) film. Within a (3x3 µm) field of view, a small square (1x1 µm) was imaged in the contact mode with sufficient loading force to remove the DNA layers. The depth of the resulting depression, relative to the surrounding film (i.e., the film thickness) was obtained by imaging in the tapping mode [30]. As shown in Fig. 2b), the 2.2 nm thick layer can be mechanically removed to show the terraces or edge steps of the intact HOPG substrate. Panel c shows a 5 ML thick layer at higher magnification, in which both the fibre-like structure of the DNA/Dap^{2+} deposits and the highly porous structure of the film are readily apparent.

B. Damage by Electron Irradiation at 10 eV

In an initial assessment of the damage induced by LEEs on DNA/Dap^{2+}complexes, multiple samples of 10 ML (22nm) thickness were irradiated with 5 nA for 90 s, at energies between 3.5 and 13.5 eV. The LEE-induced loss of the SC-form of DNA/Dap^{2+} plasmids is presented in Fig 3a and is greatest at electron energies near 10 eV, consistent with earlier results[23,24]. This loss corresponds to the formation of C- form plasmids by single strand breaks (SSBs -the major product) and L-form DNA via double strand breaks (DSBs - a minority product). Only SSBs are observed in the present experiment; the electrophoresis signal related to linear DNA fragments (i.e., DSB) and that associated with cross-links remain at the level of the background noise. Note that here the vertical axis of Fig 3a) reports an *absolute loss* of SC DNA rather than a *rate of loss* as was determined in the earlier experiments from *exposure-response* curves.[23,24]

Following initial reports[23,24], subsequent theory[33,34] and experiment[35,36] have attributed strand breaks produced at and below 10 eV as due mainly to dissociative electron attachment (DEA), a process in which an incident electron is captured by a molecule to form a molecular transient negative ion (TNI) that then dissociates into neutral and anionic fragments[37]. SSBs occur essentially by rupture of a C-O bond between sugar and phosphate groups via[33,34,36] initial electron attachment at a DNA base with subsequent electron transfer onto the backbone[38]. In addition to DEA, a *core-excited* TNI on the phosphate, may induce a SSB, if upon electron auto-detachment, a neutral dissociative state is formed[39].

C. Effect of Sample Thickness

Having confirmed that strand-break damage is at a maximum at 10 eV (Fig 3a), further measurements were performed at this energy on samples of increasing thickness, to determine cross section for this process. Exposure response curves for DNA/Dap^{2+} films of 5 ML (11nm), 7.5 ML (17.5 nm) and 10 ML (22nm) thickness are displayed in Fig 3b for irradiation at 10 eV with a J_0 of 0.39 x10^{12} electrons s^{-1} cm^{-2} . Each point represents the average of 2 measurements; the vertical bars report the standard error. In all but the earliest LEE-measurements with lyophilized plasmid DNA[23,24], the use of *high purity* DNA[22,25,26] was associated with comparatively small reductions (i.e., < 10%) in the fraction of SC-form at high electron fluence, despite a substantial effective cross section of ~$10^{-14}$$cm^2$. This apparent contradiction can be understood as due to severe film charging[22] associated with the samples' highly non-uniform thickness and surface density[20] that limit LEE penetration. Consequently, only a small percentage of the sample (< 10%) is exposed to electrons[22]. In the present experiments, the large decrease under irradiation in the percentage of SC-form indicates that DNA/Dap^{2+} films charge much less than the previous, high-purity, lyophilized samples and that electrons can thus propagate and induce damage throughout the film. In Fig.3b the exposure-response curves are, however, observed to 'plateau out' at a value close to 55%. This limit is determined by experimental details; the area of the electron beam being ~50% that of the sample. Strand break damage is only expected to occur in this fraction of the sample that is irradiated with electrons, as control experiments show that neither exposure to UV or to the vacuum environment can themselves induce SSBs.

D. Determination of Absolute Cross Section for strand break damage.

The exposure response data of Fig 3b was analysed to determine a cross section for the loss of SC DNA/Dap^{2+} complexes under electron irradiation by methods similar to the "Molecular Survival" model used to calculate damage cross sections and electron attenuation lengths in lyophilized samples[22].

In Figure 4, we consider the case of a DNA sample under electron irradiation. The sample has a thickness of "*h*+2.2 nm"; where 2.2 nm corresponds to the thickness of the permanently bound DNA monolayer and *h* is the film thickness that can be recovered by washing after irradiation. Seen from above, the sample has cross sectional area '*S*', of which a smaller area '*s*' is irradiated with an electron beam of flux 'J_0' (in no. of electrons cm^{-2} s^{-1}). Parameter '*x*' describes the depth within the film. Fraction '$P(t)$' is the percentage of undamaged plasmids remaining in the film at time '*t*'; its value at t=0 is P_0 and at long times is 'P_{min}'. In the absence of severe charging, P_{min} is determined by that fraction of the film that is not irradiated due to the mis-match in sample and electron beam diameter, i.e., $P_{min} = P_0(S-s)/S$.

The absolute cross section for the loss of SC plasmids is 'σ' while 'λ' is the attenuation length of the 10 eV electrons. Within the film, the 10 eV energy electrons undergo multiple elastic and inelastic collisions. A complete description of the electron density within the sample should include a full Monte-Carlo type analysis of the trajectory of incident electrons[40], or at least some description of the relative contributions of forward and backward scattered electrons (the two-stream approximation)[41],[42]. However by using a Poisson distribution (stochastic process) and similar to our previous analysis,[22] we propose in compliance with the relationship generally used in XPS for estimating the

Information Depth (ID) (also called penetration depth) in nanometer-scale samples, that the current density $J(x)$ decreases exponentially with penetration depth x, such that

$$J(x) = J_0 . e^{-x/\lambda} \qquad (1)$$

λ stands for the Inelastic Mean Free Path of LEEs in the films. We consider next, a horizontal slice through the sample between x and $x + dx$ and define a function $q(x,t)$ (such that $0 < q(x,t) < 1$) to represent the proportion of plasmids in the un-relaxed SC state at t in the portion 's/S' of the slice exposed to electrons. The percentage of SC plasmids $P(x,t)$ in the slice are thus:

$$P(x,t) = \left(\frac{s}{S}\right) \cdot q(x,t) \cdot P_o + \left(\frac{S-s}{S}\right) \cdot P_o \qquad (2)$$

The experimentally measurable $P(t)$ is calculated by integrating $P(x,t)$ over the recoverable thickness of the film h :

$$P(t) = \frac{1}{h} \int_0^h P(x,t) . dx \qquad (3)$$

Substituting (2) into (3) we obtain:

$$P(t) = \left(\frac{s}{S}\right) \cdot P_o \cdot \frac{1}{h} \int_0^h q(x,t)\, dx + \left(\frac{S-s}{S}\right) \cdot P_o \qquad (4)$$

The function $q(x,t)$ must satisfy the relationship

$$dq(x,t) = -\sigma . J(x) . q(x,t) dt \qquad (5)$$

which by integration with $q(x,0)=1$, has as a solution:

$$q(x,t) = e^{-\sigma . J(x) . t} = e^{-\sigma J_0 . e^{-x/\lambda} . t} \qquad (6)$$

Considering that as t tends to infinity, $q(x,t)$ tends to 0 and $P_{min} = P_0(S-s)/S$.

We see by inspection of (4) that equation (4) can be rewritten as:

$$P(t) = (P_o - P_{min}) \cdot \left(\frac{1}{h}\int_0^h e^{-\sigma \cdot J_o \cdot e^{-x/\lambda} \cdot t}\, dx\right) + P_{min} \qquad (7)$$

At short times, (7) simplifies to a linear function. In our previous analysis of strand break damage in lyophilized films[22], a very pronounced dependence on film thickness was observed and λ and σ were determined independently by consideration of data obtained at low electron fluence alone.[22] However, it is apparent in Figure 3b that the three exposure response curves are remarkably similar, indicating that the attenuation length in the present experiments is greater than the range of film thicknesses studied and confounds our previous approach. Fortunately (7), can be evaluated numerically and Levenberg-Marquardt optimization[43], further permits the most probable values of P_0, P_{min}, σ and λ to be determined at each film thickness. It was found that the optimal values depend slightly on the initial seed values. Multiple fitting sessions (between 65 and 90 instances) using randomized seed values were thus performed on each dataset to obtain a population of λ, σ, P_0, and P_{min} values, that fit well the experimental data at each thickness. While average values of P_0 and P_{min} were relatively constant, (for example those for P_{min} were determined as 56.85%, 55.62% and 56.03% for 5 ML, 7.5 ML and 10 ML films respectively with standard deviations < 0.8%) larger variations in λ and σ were observed. Figure 5 plots pairs of λ and σ values for the three films. Excluded from the plot are a small number of `unphysical` solutions (e.g., negative values for λ or $\lambda > 10^{-6}$ m). Distinct but overlapping distributions can be seen at each thickness. Mean values for λ and σ and their standard deviations were calculated at each thickness and combined to obtain weighted mean values (and associated uncertainties) for the ensemble of experiments. The results are tabulated in Table 1; The mean cross section σ for loss of

SC-form (and its conversion into the C-state) is (3.0 ±0.3) x 10^{-14} cm^2 at 10 eV while λ, was determined to be 14.1±5.4 nm. The mean values for σ and λ have been used to generate the fitted curves of Figure 3.

Formally, this cross section describes the probability, at an incident electron energy 10 eV, of strand-break damage in the particular DNA/Dap^{2+} complexes used in these experiments. A more transportable cross section can be obtained by normalizing the cross section to the number of base pairs in the pUC21 plasmid (i.e., 3151bp). The resulting cross section per base σ_b, has a value of (4.8 ±0.5) x 10^{-18} cm^2 and is also included in table 1. This latter can be compared to that measured in lyophilized samples of varying thickness, of *pure* DNA (plasmid pGEM-3Zf(–), 3197 bp) (5.9 ± 1.9 x 10^{-18} cm^2)[22]. It thus appears that, within the reported experimental uncertainties, the absolute cross section for SC-form loss is similar for both pure DNA plasmids and the DNA/Dap^{2+} complexes.

The λ determined here (14.1±5.4) nm is somewhat, but not significantly, larger than that found in lyophilized samples (10.4±5.4, ref.22). In those earlier experiments there was evidence that film charging under LEE irradiation, decreased the λ values obtained for thicker samples. In the absence of severe charging, as is the case in the present experiments, it is perhaps unsurprising to find a longer λ,. We should perhaps also consider the porosity of the present samples evident in Figure 2. It seems possible that LEEs might travel easily through large thicknesses due to the nano-metric holes present inside these films. It is possible that experiments involving with a wider range of film thicknesses could improve accuracy in the determination of λ (and also σ),

However we are presently unable to produce DNA/Dap^{2+} films of thicker than 15 ML with acceptable precision. Our preliminary studies [44] have shown that the thicker the film the larger the standard deviation associated with the mean thickness, as measured by AFM; with thicknesses > 15 ML, this deviation becomes greater than 20-30% of the thickness itself. The thicknesses used in the present study must then be seen as a best experimental compromise. Experiments to evaluate the attenuation length of low energy photoelectrons through DNA/Dap^{2+} films of various thicknesses are in progress.

In contrast to earlier experiments, the present preliminary results do not report the formation of linear DNA via DSBs. This surprising absence and its relationship to the presence of Dap^{2+} will be a subject of future study. It is possible that the presence of Dap^{2+} perturbs in some way inter-strand electron transfer which is believed to be required for the induction of DSB by LEEs and TNIs[39].

IV. CONCLUSION

In conclusion, we find that highly organized DNA films in which DNA plasmids are complexed with 1,3-diaminopropane[30] are suitable for quantitative LEE irradiation studies. Such samples have allowed the determination of an absolute cross section for electron induced damage at 10 eV, specifically the loss of SC plasmids. The value is consistent with measurements obtained in lyophilized samples[22]. Due to their chemical composition which includes ionized diamines (Figure 1), these samples can serve as useful tools to evaluate how LEE-DNA interactions are modified by material bound to DNA in cell nuclei, such as histones. Furthermore, they may provide useful quantitative information for more accurate simulations of LEE damage in real-world biological environments. Comparing the present CS measurement to those obtained from pure DNA

films, we find that binding protein-like NH_3^+ group to DNA does not significantly modify the total cross section for loss of the super-coiled structure.

Tables

Table 1. Values of attenuation length λ, and cross section σ for loss of SC DNA at 10 eV (and respective errors $\delta\lambda$ and $\delta\sigma$) as determined from the exposure response data of Figure 3b. For each curve, multiple Levenberg-Marquardt optimizations with randomized initial conditions, were used to generate populations of optimal λ and σ values. The mean of these populations and their standard deviations are used to represent the λ, σ and their respective errors at each thickness. The final values of these parameters are the weighted means of results from the three thicknesses. The cross section per base σ_b and its associated error $\delta\sigma_b$ which are calculated from the mean σ and its error are also tabulated.

Thickness (ML)	h (nm)	λ (nm)	$\delta\lambda$ (nm)	σ (10^{-14} cm^2)	$\delta\sigma$ (10^{-14} cm^2)	σ_b (10^{-18} cm^2)	$\delta\sigma_b$ (10^{-18} cm^2)
5	8.8	9.2	6.1	4.8	1.2		
7.5	15.3	61.7	45.1	2.7	0.5		
10	19.8	29.9	12.2	3.0	0.4		
Weighted Mean		14.1	5.4	3.0	0.3	4.8	0.5

Figures.

Figure 1. a) Doubly protonated 1-3 diaminopropane (Dap^{2+}) at neutral pH. b) Schematic representation of .DNA-Dap^{2+} complexes binding to HOPG. Dap^{2+} screens the DNA negatively charged phosphate groups and permits precipitation onto the hydrophobic surface. Linking by Dap^{2+} between phosphates on adjacent strands secures additional layers.

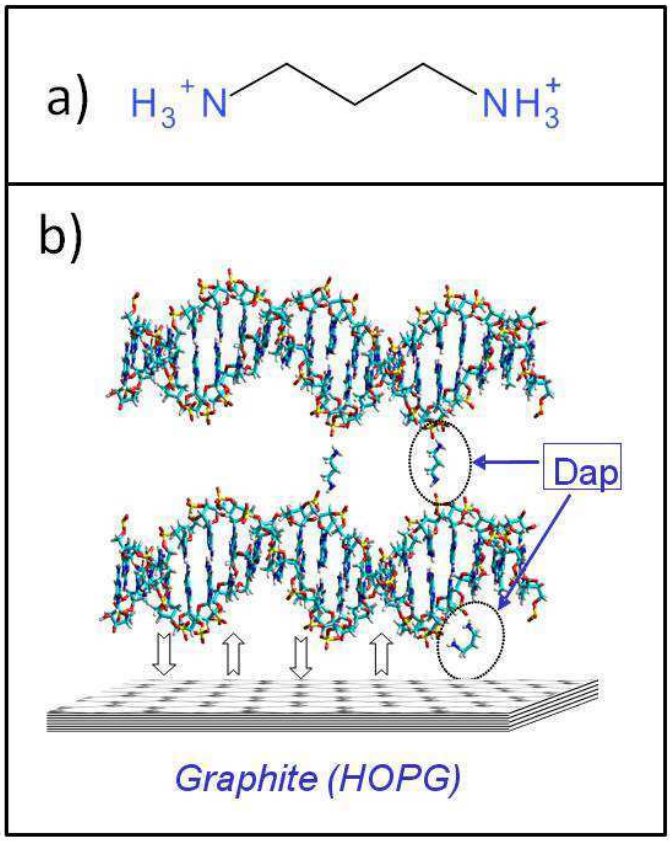

Figure 2 AFM measurement of the thickness of a DNA layer. a) Scratching with the tip of the AFM makes a depression in the DNA/Dap^{2+} surface, the depth of which corresponds to the film thickness H; b) Measurement of the thickness of the insoluble first monolayer (2.2 nm); c) High resolution image of the porous film structure.

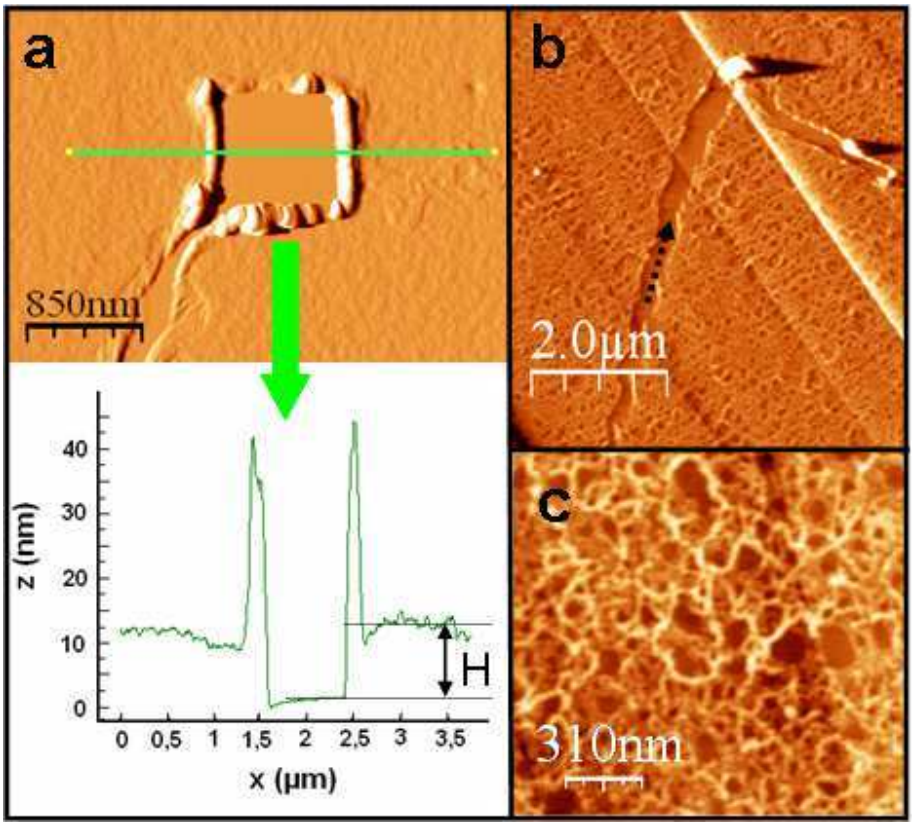

Figure 3 (a) Percentage loss of the SC configuration of DNA as a function of incident electron energy after irradiation of a DNA/Dap^{2+} film of 20 nm (10ML) for a period of 1.5 minutes under a current density of 0.39 x 10^{12} electrons.cm^{-2}.s^{-1}. The dotted line is to guide the eye. **(b)** Percentage of DNA/Dap^{2+} sample remaining in the SC state, as function of irradiation time at 10 eV, for films of three different thicknesses (5, 7.5 and 10 ML). Solid curves correspond to optimal exponential fits to the data. See text for details.

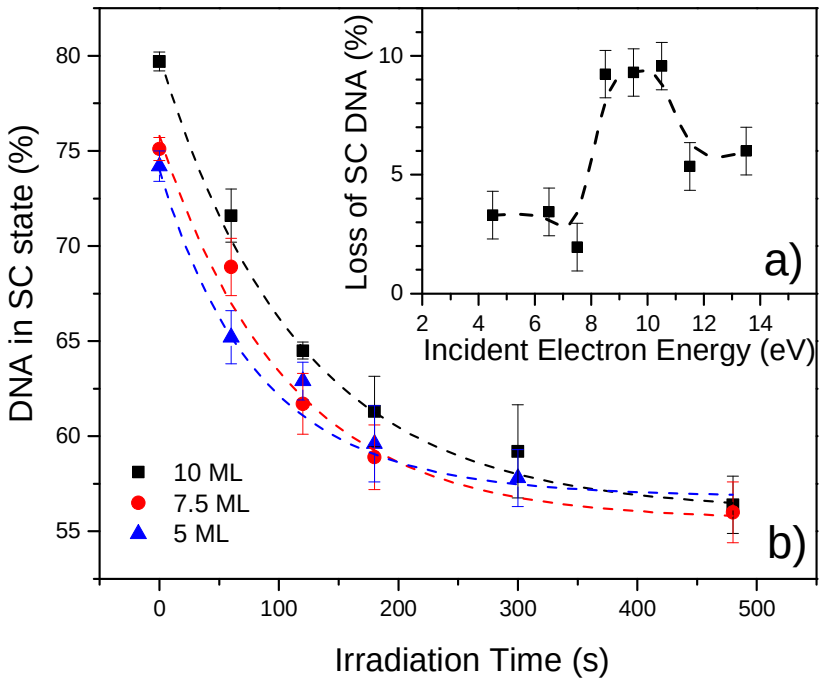

Figure 4 Schematic of our model system for determining the fraction of undamaged plasmid DNA '*P*(*t*)' as a function of the cross section 'σ' for damage and the electron attenuation length 'λ'.

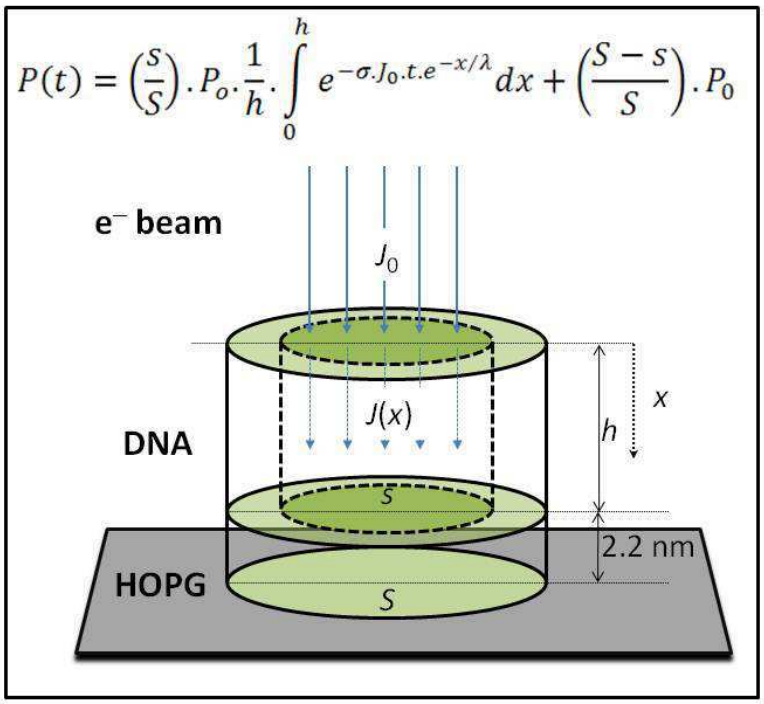

Figure 5 Graph showing the distribution of optimized solutions of equation (7) for attenuation length 'λ' and cross section 'σ', for each of the three film thicknesses irradiated with 10 eV electrons (Experimental data presented in Fig 3b). Each point represents a Levenberg-Marquardt optimized solution for σ and λ derived from randomized seed values for P_0, P_{min}, σ and λ. Excluded from the plot are a small number of `unphysical` solutions (e.g., negative values for λ or λ >10^{-6} m).

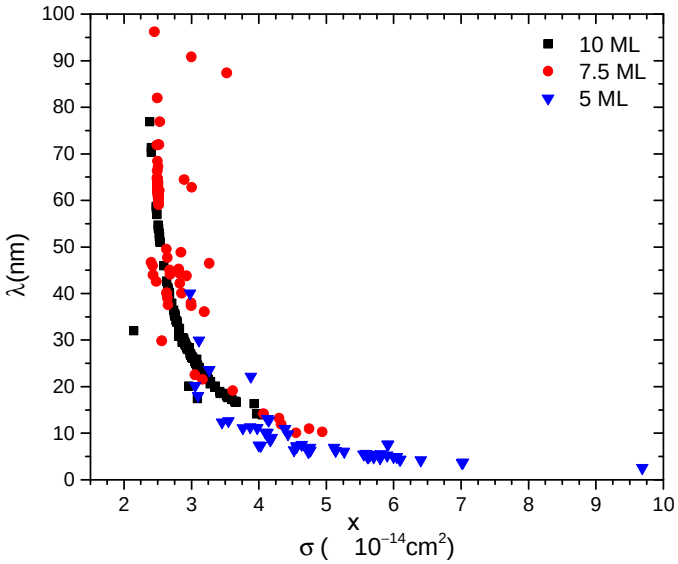

[1] S. M. Pimblott and J. A. LaVerne, *Radiat. Phys. Chem.* **76**, 1244-1247 (2007).

[2] M. Dingfelder, *Radiation Protection Dosimetry* **122**, 16-21 (2006).

[3] H. Nikjoo, S. Uehara, D. Emfietzoglou and F. A. Cucinotta, *Radiat.Measur.***41**, 1052-1074 (2006).

[4] I. Rozum, P. Limao-Vieira, S. Eden, J. Tennyson and N. J. Mason, *J. Phys. Chem. Ref. Dat.* **35**, 267-84 (2006).

[5] T.-.Kim, J. -. Lee and M. -. Lee, *Radiat. Phys. Chem.* **76**, 1037-1041 (2007).

[6] T. E. Madey, R. E. Johnson and T. M. Orlando, *Surf Sci* **500**, 838-858 (2002).

[7] M. Durante and F. A. Cucinotta, *Nat Rev Cancer* **8**, 465-472 (2008).

[8] I. Baccarelli, I. Bald, F. A. Gianturco, E. Illenberger and J. Kopyra, *Physics Reports*. **508**, 1-44 (2011).

[9] W. Friedland, M. Dingfelder, P. Kundrát and P. Jacob, *Mutat. Res.* **711**, 28-40 (2011).

[10] H. Nikjoo, D. Emfietzoglou, R. Watanabe and S. Uehara, *Radiat. Phys. Chem.* **77**, 1270-1279 (2008).

[11] L. Zhang and Z. Tan, A new calculation on spectrum of direct DNA damage induced by low-energy electrons. *Radiat. Environ. Biophys.* **49**, 15-26 (2010).

[12] Z. Tan, Y. Xia, X. Liu, M. Zhao, Y. Ji, F. Li and B. Huang, Cross sections of electron inelastic interactions in DNA. *Radiat. Environ. Biophys.* **43**, 173-182 (2004).

[13] Z. Tan, Y. Xia, X. Liu, M. Zhao, Y. Ji, F. Li and B. Huang, *Appl. Phys. A: Mat. Sci. Proc.* **81**, 779-786 (2005).

[14] P. Mozejko and L. Sanche, *Radiat. Phys. Chem.* **73**, 77-84 (2005).

[15] P. Mozejko and L. Sanche, *Radiat. Environ. Biophys.* **42**, 201-211 (2003).

[16] M. Michaud and L. Sanche , *Phys. Rev. A* **36**, 4672-83 (1987).

[17] M. Michaud, A. T. Wen and L. Sanche, *Radiat. Res.* **159**, 3-22 (2003).

[18] TL Merrigan, C.A. Hunniford, D.J.Timson, M. Catney M and RW McCullough,. *Euro. Phys. J. D* **60,** 163-9 (2010).

[19] I. Bald, I. Dąbkowska and E. Illenberger, *Angewandte Chemie International Edition* **47**, 8518-8520 (2008).

[20] M. A. Śmiałek, R. Balog, N. C. Jones, D. Field and N. J. Mason, *Euro. Phys. J. D* **60**, 31-36 (2010).

[21] M. Śmiałek, N. Jones, R. Balog, N. Mason and D. Field, *Euro. Phys. J. D* **62**, 197-203 (2011).

[22] M. Rezaee, P. Cloutier, A. D. Bass, M. Michaud, D. J. Hunting, and L. Sanche , *Phys. Rev. E* **86**, 031913 (2012)

[23] B. Boudaiffa, P. Cloutier, D. Hunting, M. A. Huels and L. Sanche, *Science* **287**, 1658-60 (2000).

[24] B. Boudaiffa, P. Cloutier, D. Hunting, M. A. Huels and L. Sanche, *Radiat. Res.* **157**, 227-34 (2002).

[25] F. Martin, P. D. Burrow, Z. Cai, P. Cloutier, D. Hunting and L. Sanche, *Phys. Rev. Lett.* **93**, 068101-1 (2004).

[26] R. Panajotovic, F. Martin, P.Cloutier, D. Hunting, and L. Sanche. *Radiat. Res.* **165**, 452 (2006).

[27] E. Larqué, M. Sabater-Molina and S. Zamora, *Nutrition* **23**, 87-95 (2007).

[28] E. Koculi, D. Thirumalai and S. A. Woodson, *J. Mol. Biol.* **359**, 446-454 (2006).

[29] H. Cao and G. B. Schuster, *Bioconjug. Chem.* **16**, 820-826 (2005).

[30] O. Boulanouar, A. Khatyr, G. Herlem, F. Palmino, L. Sanche and M. Fromm, *J. Phys. Chem. C* **115**, 21291-21298 (2011).

[31] V. A. Bloomfield, D. M. Crothers and I. J. Inoco, *Nucleic acids: Structures, properties, and functions.* Sausalito CA, University Science Books, 2000.

[32] O. Boulanouar, M. Fromm, C. Mavon, P. Cloutier, L. Sanche. *J. Chem. Phys.* accepted (2013).

[33] R. Barrios, P. Skurski and J. Simons, *J. Phys. Chem. B,* **106**, 7991, (2002).

[34] X. Li, M. D. Sevilla and L. Sanche, *J. Am. Chem. Soc.*, **125**, 13668, (2003).

[35] X. Pan, P. Cloutier, D. Hunting, L. Sanche, *Phys. Rev. Lett. 90*, 208102. (2003).

[36] Y. Zheng, P. Cloutier, D. J. Hunting, L. Sanche and J. R. Wagner, *J. Am. Chem. Soc.*, **127**, 16592, (2005).

[37] R. Hashemi, A. Kuhn, and E. Illenberger, *Int. J. Mass. Spectrom. Ion. Process.* **100**, 753 (1990).

[38] J. Gu, J. Wang, J. Leszczynski. *Nuc. Acids Res.* **38,** 5280, (2010).

[39] Z. Li, P. Cloutier, L. Sanche and J. R. Wagner, *J. Phys. Chem. B.* **115**, 13668 (2011)

[40] T. Goulet, E. Keszei, and J.-P. Jay-Gerin, Phys. Rev. A **37**, 2176 (1988); E. Keszei, T. Goulet, and J.-P. Jay-Gerin, ibid.**37**, 2183 (1988);**41**, 6006 (1990)

[41] P. J. Chantry, A. V. Phelps, and G. J. Schulz, Phys. Rev. **152**, 81–98 (1966)

[42] M. Michaud and L. Sanche, Phys. Rev. B **30**, 6067 (1984)

[43] W. H. Press , S. A. Teukolsky, W. T. Vetterling, B. P. Flannery Numerical Recipes: The Art of Scientific Computing, Third Edition (Cambridge University Press, Cambridge, UK, 2007)

[44] O. Boulanouar, Ph D thesis, Université de Franche-Comté, 2011